Supporting Information

Structure, Composition and Electrochemical Performance Analysis of Fluorophosphates from Different Synthetic Methods: Is It Really $Na_3V_2(PO_4)_2F_3$ Synthesized?

Long Li[1], Jing Zhao[1,+], Hongyang Zhao[1], Yuanyuan Qin[1], Xiaolong Zhu[2], Hu Wu[1], Zhongxiao Song[2], Shujiang Ding[1,*]

[1]School of Chemistry, Xi'an Key Laboratory of Sustainable Energy Materials Chemistry, State key laboratory of Electrical Insulation and Power Equipment, Xi'an Jiaotong University, Xi'an 710049, P. R. China

[2]State Key Laboratory for Mechanical Behavior of Materials, Xi'an Jiaotong University, Xi'an, Shaanxi, 710049, China

[*]*Corresponding author: dingsj@xjtu.edu.cn* (Shujiang Ding) L. Li and J. Zhao contributed equally to this work.

Supplementary Figure 1.

Figure S1 XPS spectra of C 1s for the composites synthesized by sol-gel method.

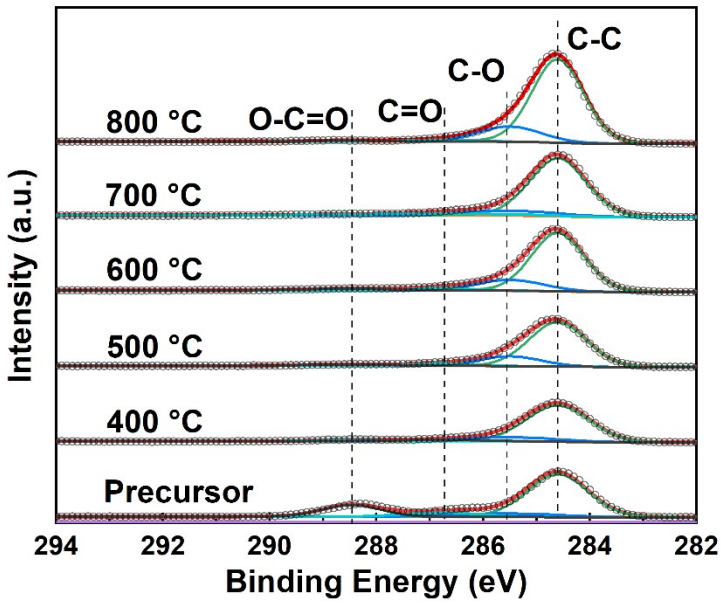

Supplementary Figure 2.

Figure S2 XRD patterns of gel precursor.

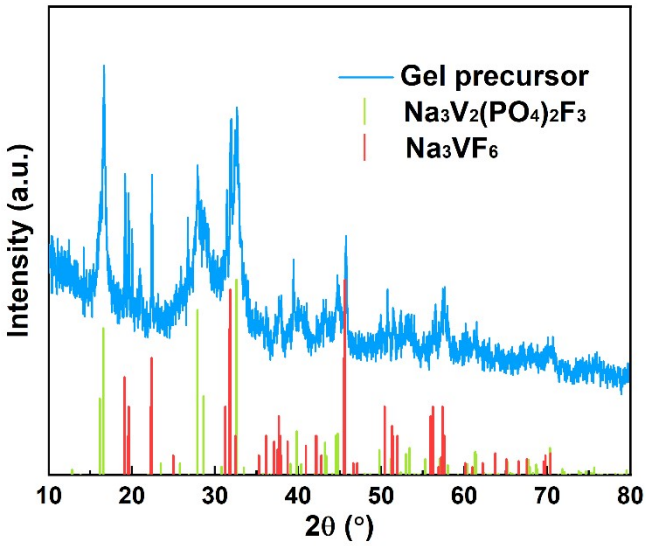

The NVPF was prepared by a general sol-gel method at 600 ºC in Ar atmosphere. Figure S2 show XRD patterns of the gel precursor, confirming the NVPF grains have been formed after the sol-gel process.

Supplementary Figure 3.

Figure S3 SEM images (a)-(e) and corresponding EDS analysis (f) of gel precursor obtained at different temperatures; the inserts show the particle size distribution of as prepared samples.

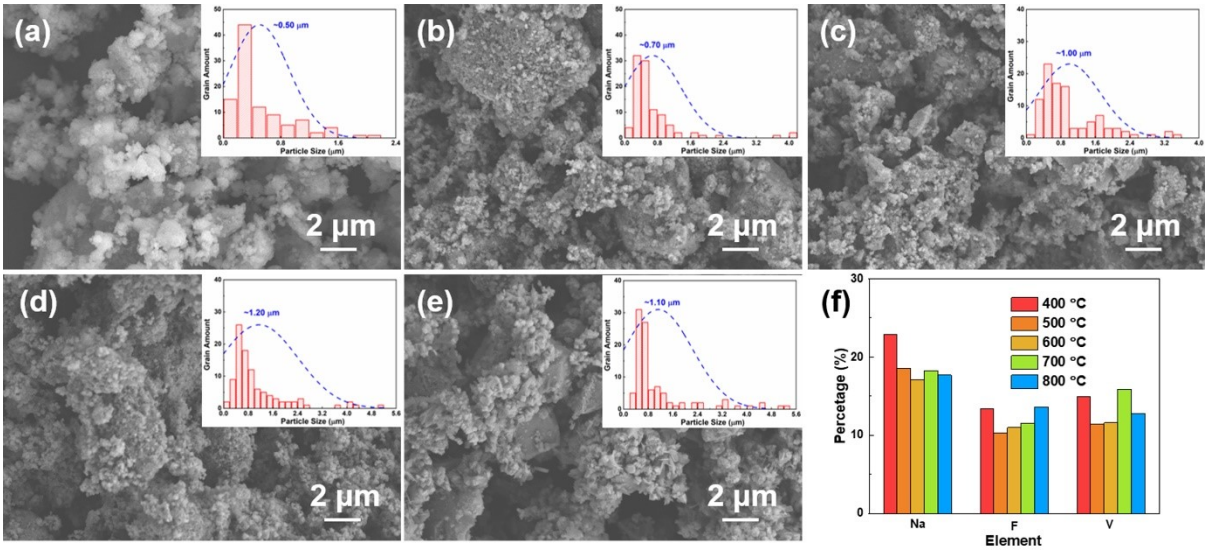

Supplementary Figure 4.

Figure S4 (a)~(f) The EDS (Na, P, O, V and F) analysis of NVPF-SG400.

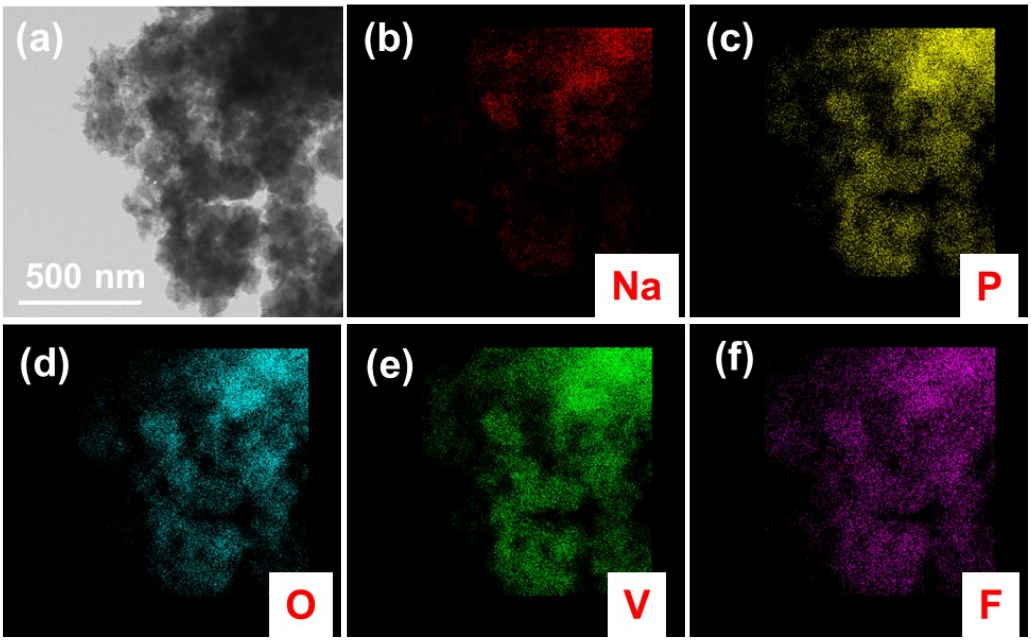

Supplementary Figure 5.

Figure S5 T(a)~(f) The EDS (Na, P, O, V and F) analysis of NVPF-SG600.

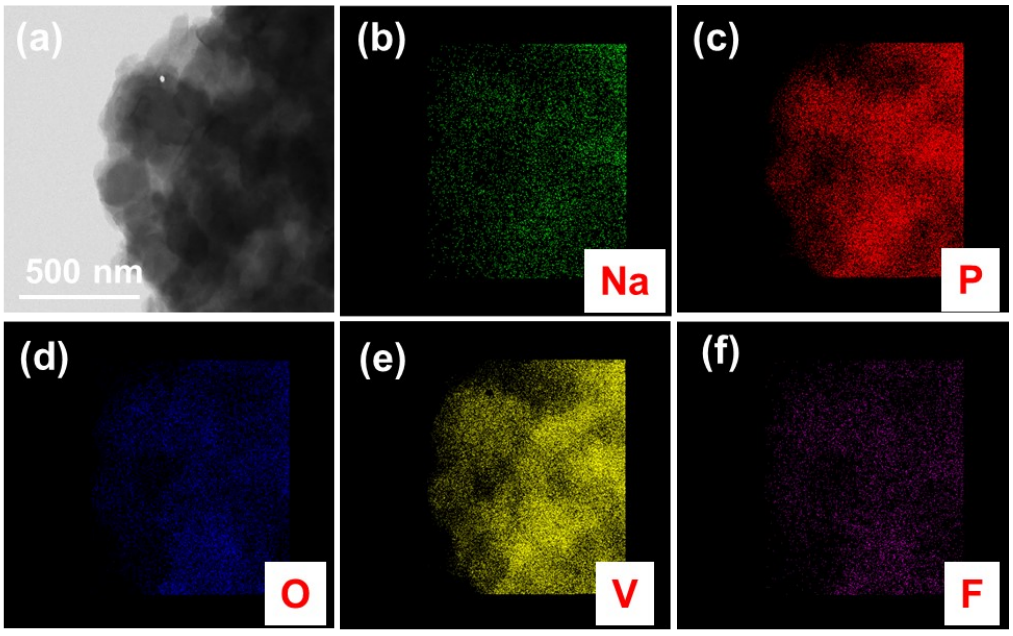

Supplementary Figure 6.

Figure S6 (a)~(f) The EDS (Na, P, O, V and F) analysis of NVPF-SG800.

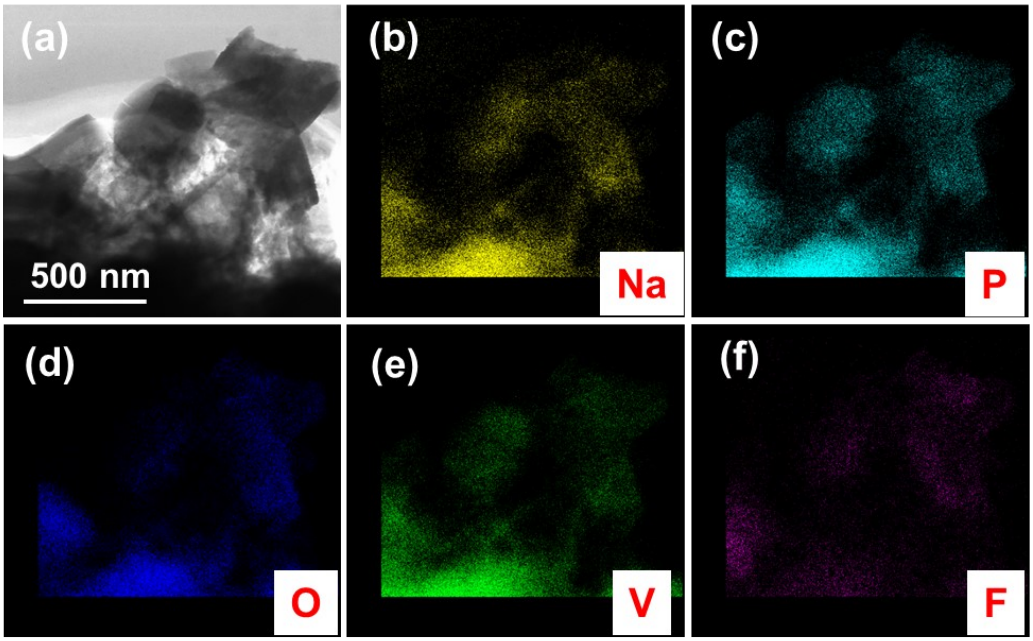

Supplementary Figure 7.

Figure S7 the TGA/DSC curves of the NaF and VPO_4 mixture annealing from 50 to 900 ºC.

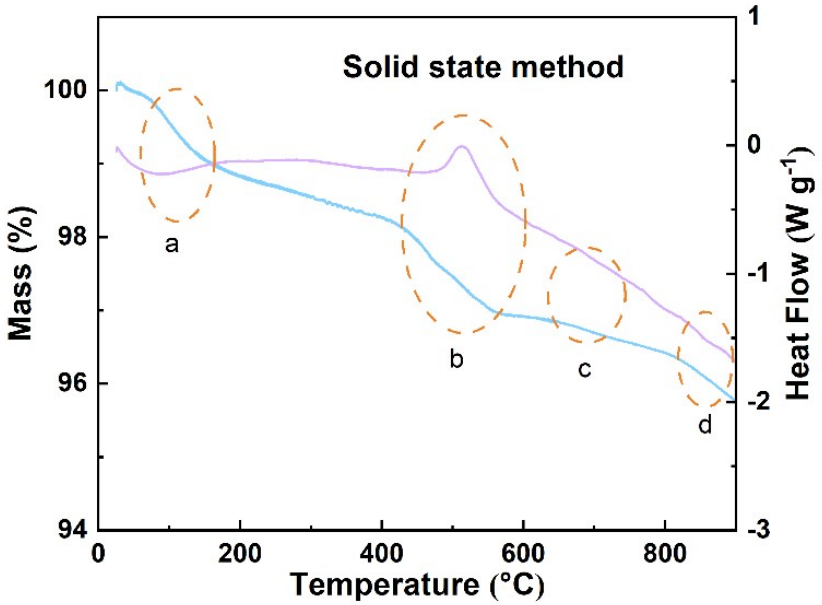

Supplementary Figure 8.

Figure S8 SEM images (a)~(d) of NVPF synthesized at 500, 600, 700 and 800 ºC by solid-state method; the inserts show the particle size distribution of as prepared samples.

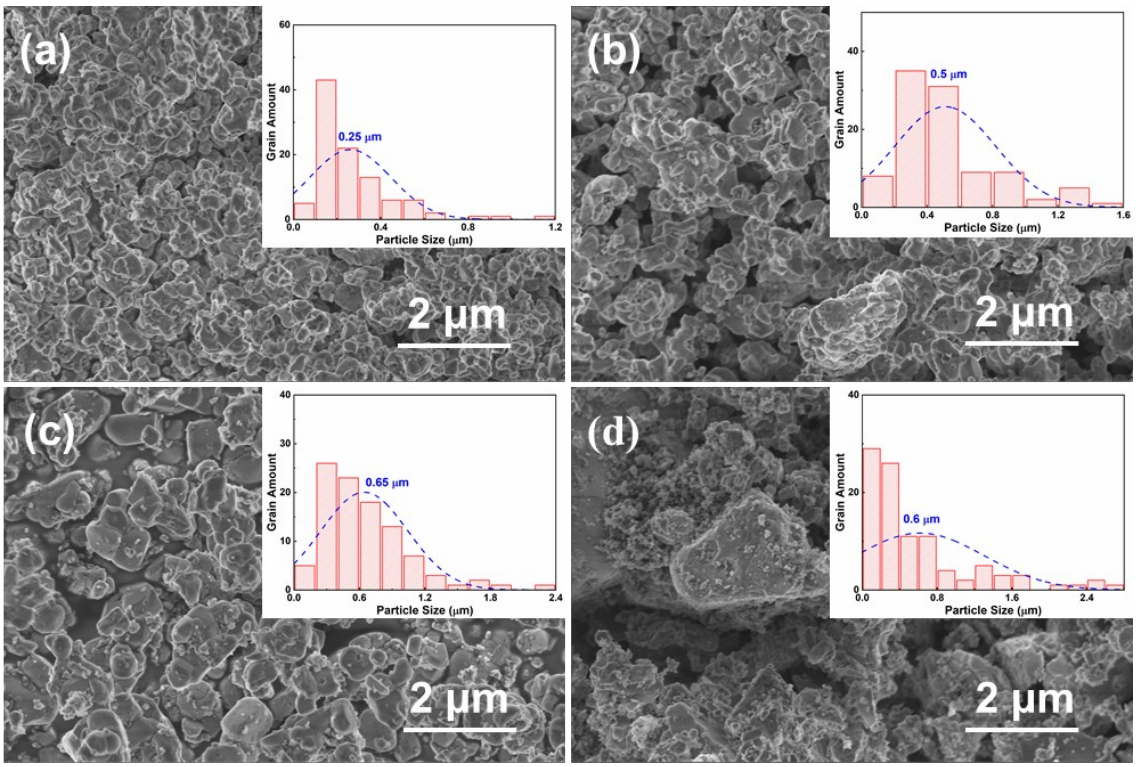

Supplementary Figure 9.

Figure S9 The EDS element analysis of raw material and NVPF composite obtained by solid-state method at 500-800 ºC.

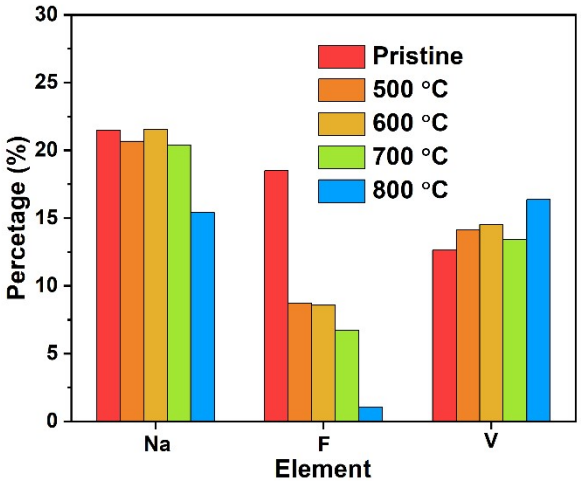

Supplementary Figure 10.

Figure S10 TEM images and SEAD patterns of NVPF-SS600 (a)~(c) and NVPF-SS800 (d)~(f) obtained by solid-state method.

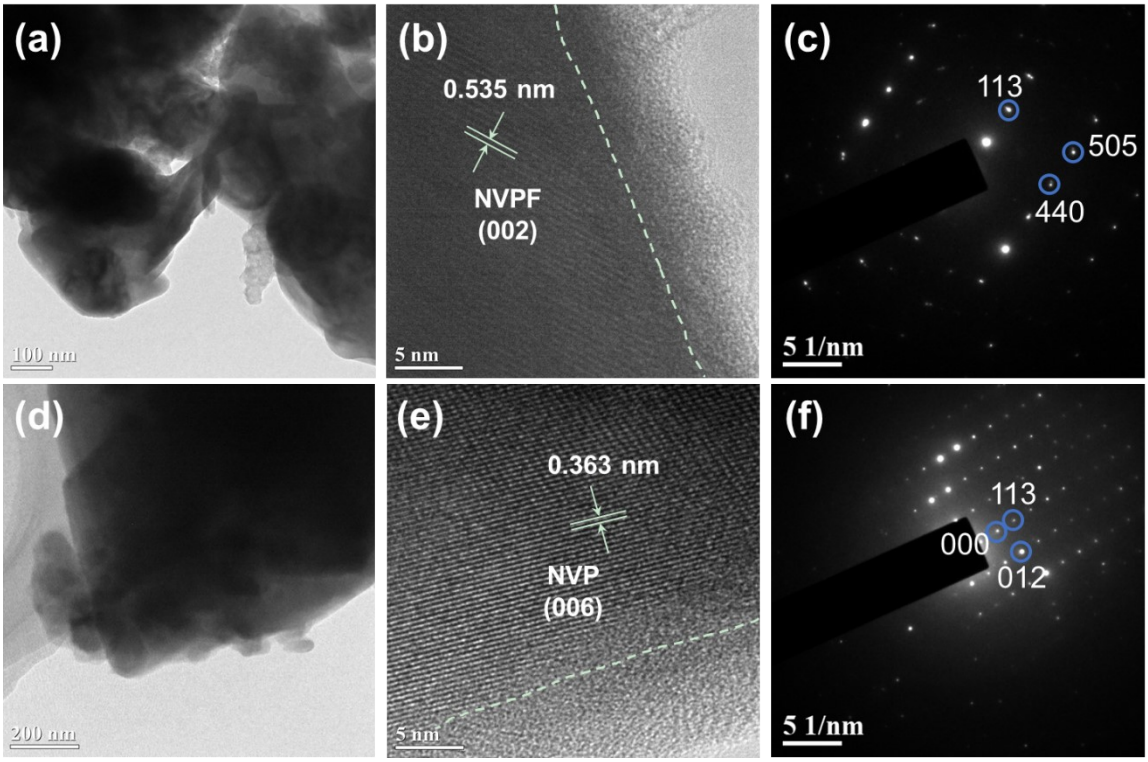

Supplementary Figure 11.

Figure S11 TEM images (a) and SEAD pattern (b) of single crystal pristine NVPFO obtained by hydrothermal method.

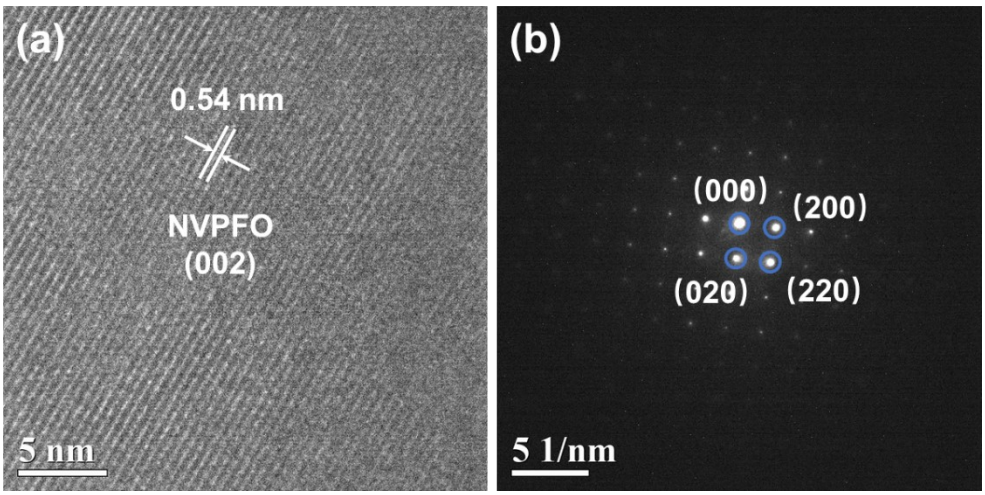

Supplementary Figure 12.

Figure S12 TEM images of pristine NVPFO (a) and the composites annealed at 400, 600 and 800 (b)~(d).

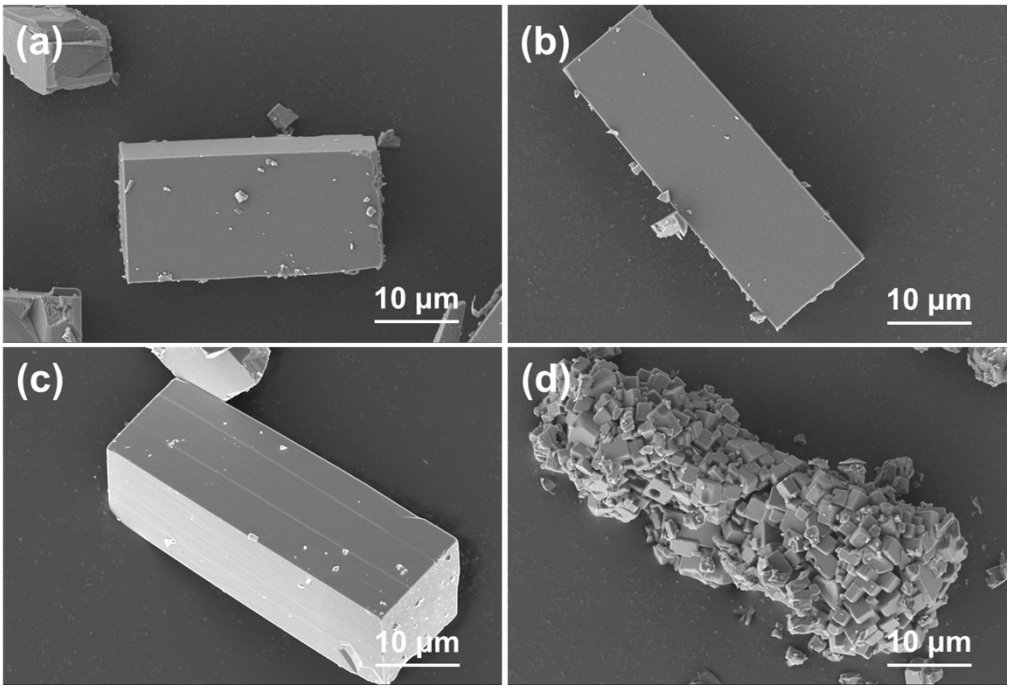

Supplementary Figure 13.

Figure S13 The EDS element analysis of pristine NVPF obtained by solid-state method annealed at 400, 600 and 800 ºC.

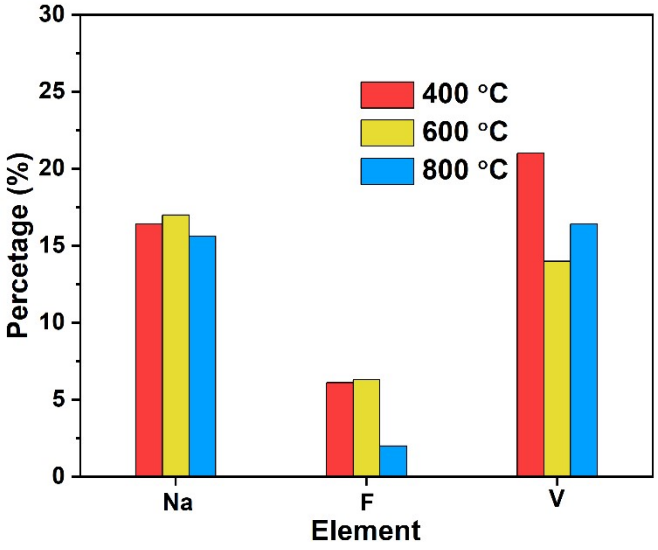

Supplementary Figure 14.

Figure S14 XRD pattern of the as-prepared NVPF-SS600, NVPF-SG600 and NVOPF-600 samples.

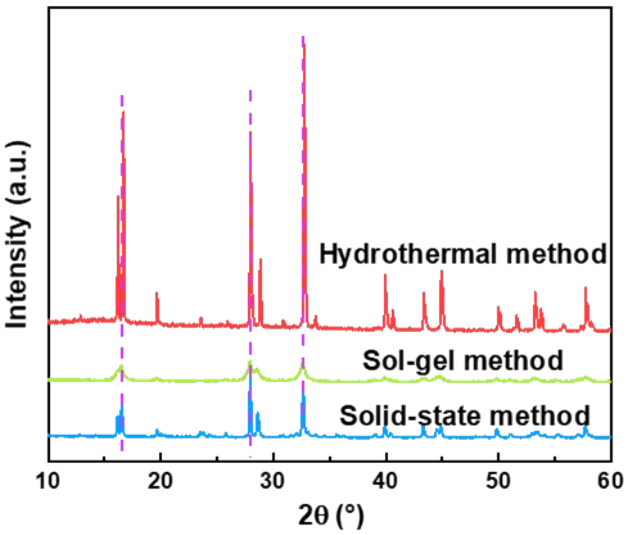

As displayed in Figure S14, the peak positions of XRD patterns in the as-prepared NVPF-SS600, NVPF-SG600 and NVOPF-600 are almost the same, while the valence of V element and V–O stretching vibration are gradually increased, signifying the increasing substitution of O atoms in F sites.

Supplementary Figure 15.

Figure S15 XRD patterns of NVPF-SG-400 (a), NVPF-SG-600 (b) and NVPF-SG-800 (c) electrodes after 0 and 100 cycles.

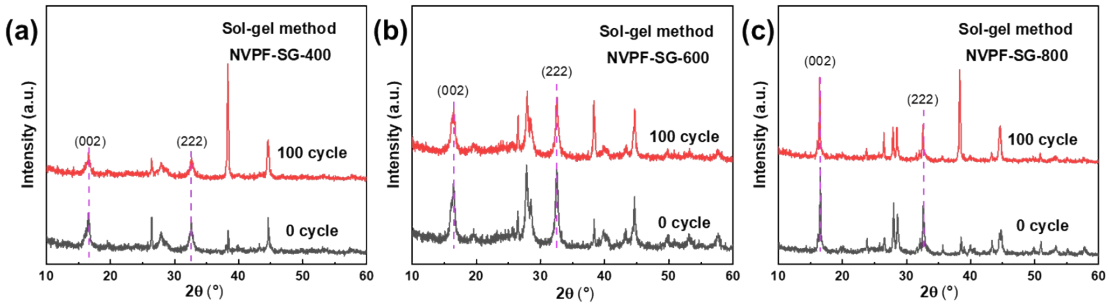

Supplementary Figure 16.

Figure S16 XRD patterns of NVPF-SS-600 (a) and NVPF-SS-800 (b) electrodes after 0 and 100 cycles.

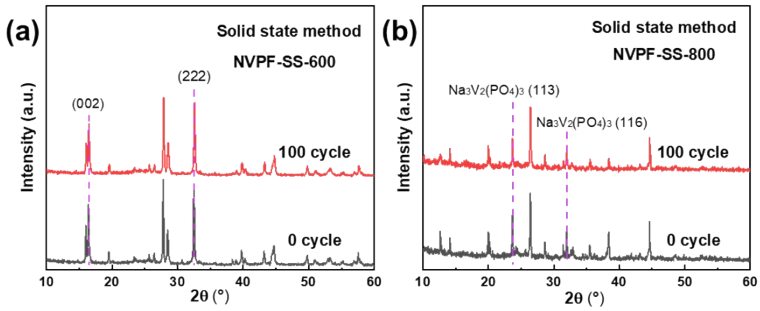

Supplementary Figure 17.

Figure S17 XRD patterns of NVOPF-400 (a), NVOPF-600 (b) and NVOPF-800 (c) electrodes after 0 and 100 cycles.

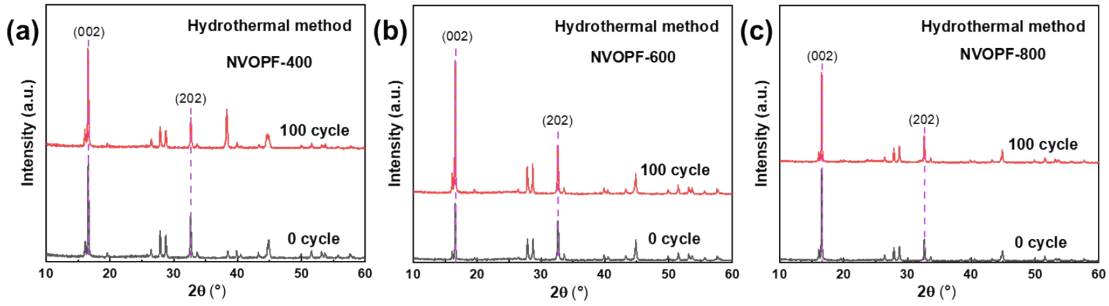

Supplementary Figure 18.

Figure S18 SEM images of NVPF-SG-400 (a, d), NVPF-SG-600 (b, e) and NVPF-SG-800 (c, f) electrodes after 0 and 100 cycles.

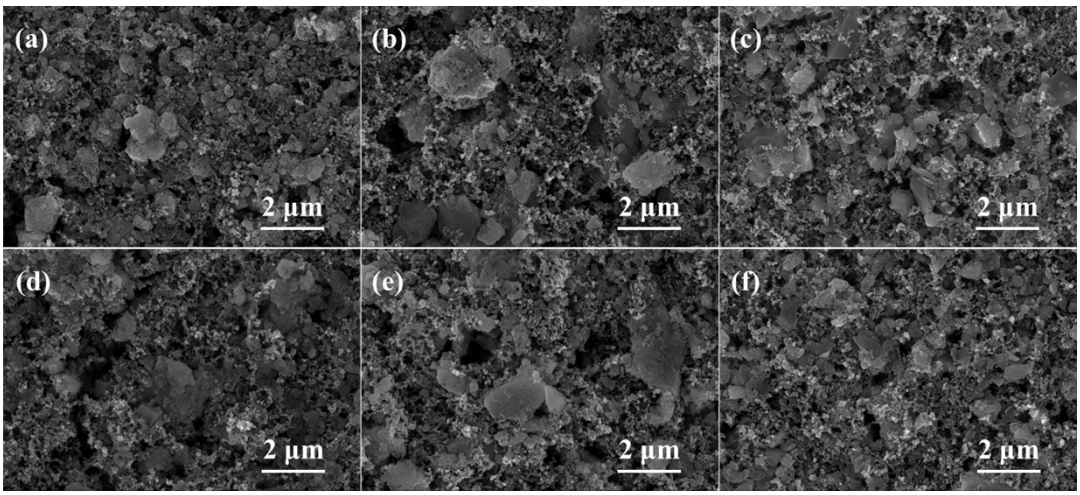

Supplementary Figure 19.

Figure S19 SEM images of NVPF-SS-600 (a, c) and NVPF-SS-800 (b, d) electrodes after 0 and 100 cycles.

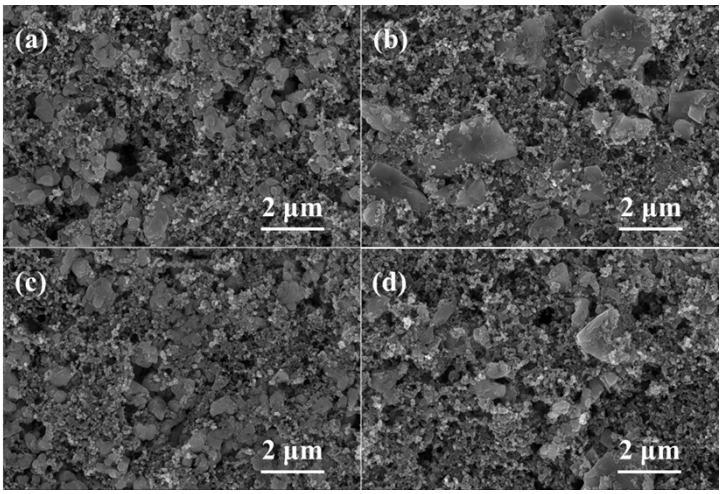

Supplementary Figure 20.

Figure S20 SEM images of NVOPF-400 (a, d), NVOPF-600 (b, e) and NVOPF-800 (c, f) electrodes after 0 and 100 cycles.

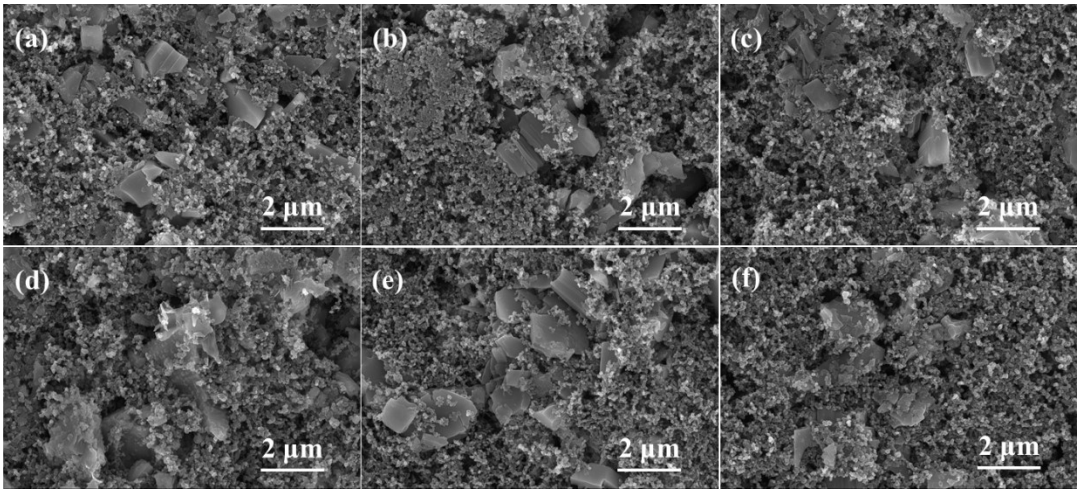

Table R1 List of recent works on vanadium based fluorophosphate cathode for SIBs

Materials	Potential window **(V)**	Initial discharge capacity (mA h g^{-1})	Rate (C)	Capacity (mAh g^{-1})	Capacity attenuation per cycle	Publication year [Ref.]
$Na_3(VPO_4)_2F_3$	2.5-4.3	~104	2	~93.6 after 1200 cycles	0.83E-4	2015 [1]
$Na_3(VOPO_4)_2F$	2.5-4.3	~103	2	101.9 after 1200 cycles	0.83E-4	2015 [1]
$Na_3V_2O_2(PO_4)_2F$-MWCNT	2.0-4.5	110.0	0.1	98 after 120 cycles	9.09E-4	2016 [2]
$Na_3V_{1.95}Y_{0.05}(PO_4)_2F_3$/C	2.0-4.5	124.1	1	111.8 after 200 cycles	4.94E-4	2017 [3]
$Na_3V_2O_2(PO_4)_2F$@RGO	2.0-4.5	120.4	0.5	107.9 after 200 cycles	5.15E-4	2017 [4]
$Na_3V_2(PO_4)_2F_3$/C@RGO	2.5-4.3	124.5	1	108.3 after 700 cycles	1.89E-4	2018 [5]
$Na_3V_2(PO_4)_2F_3$–SWCNT-2	2.5-4.3	111.4	0.5	102.9 after 100 cycles	7.60E-4	2019 [6]
$Na_3V_2(PO_4)_2F_3$@rGO	2.0-4.3	119.0	0.5	119 after 100 cycles	/	2020 [7]
$Na_3V_2(PO_4)_2F_3$@C-3	2.0-4.3	102.0	1	95.5 after 310 cycles	2.06E-4	2020 [8]
$Na_3V_2(PO_4)_2F_3$@rGO	2.0-4.3	122.3	1	104.1 after 500 cycles	2.97 E-4	2020 [9]
$Na_3V_2(PO_4)_2F_3$-$Mn_{0.02}$	2.0-4.3	~118	1	~96.6 after 1000 cycles	1.81 E-4	2021 [10]
$Na_3V_2O_2(PO_4)_2F$ @C/CNFs-PA	2.0-4.3	105.0	2	93.3 after 500 cycles	2.22 E-4	2021 [11]
$Na_3V_2(PO_4)_2F_3$-Zr-0.02/NC	2.0-4.5	119.2	0.5	~103 after 200 cycles	6.8E-4	2022 [12]
$Na_3V_2O_2(PO_4)_2F$	2.5-4.3	117.32	1	115.48 after 400 cycles	0.39E-4	This work

References

1. Y. Qi, L. Mu, J. Zhao, Y.-S. Hu, H. Liu and S. Dai, *Angew. Chem. Int. Ed.*, 2015, **54**, 9911-9916.
2. P. R. Kumar, Y. H. Jung, J. E. Wang and D. K. Kim, *J. Power Sources*, 2016, **324**, 421-427.
3. W. Liu, H. Yi, Q. Zheng, X. Li and H. Zhang, *J. Mater. Chem. A* 2017, **5**, 10928-10935.
4. Y. Yin, F. Xiong, C. Pei, Y. Xu, Q. An, S. Tan, Z. Zhuang, J. Sheng, Q. Li and L. Mai, *Nano Energy*, 2017, **41**, 452-459.
5. L. Li, Y. Xu, X. Sun, S. He and L. Li, *Chem. Eng. J.*, 2018, **331**, 712-719.
6. S. Liu, L. Wang, J. Liu, M. Zhou, Q. Nian, Y. Feng, Z. Tao and L. Shao, *J. Mater. Chem. A* 2019, **7**, 248-256.
7. F. Li, Y. Zhao, L. Xia, Z. Yang, J. Wei and Z. Zhou, *J. Mater. Chem. A* 2020, **8**, 12391-12397.
8. Y. Li, X. Liang, G. Zhong, C. Wang, S. Wu, K. Xu and C. Yang, *ACS Appl. Mater. Interfaces*, 2020, **12**, 25920-25929.
9. L. Zhu, Q. Zhang, D. Sun, Q. Wang, N. Weng, Y. Tang and H. Wang, *Materials Chemistry Frontiers*, 2020, **4**, 2932-2942.
10. Z.-Y. Gu, J.-Z. Guo, Z.-H. Sun, X.-X. Zhao, X.-T. Wang, H.-J. Liang, B. Zhao, W.-H. Li, X.-M. Pan and X.-L. Wu, *Small*, 2021, **17**, 2102010.
11. X. Li, S. Jiang, S. Li, J. Yao, Y. Zhao, T. Bashir, S. Zhou, S. Yang, W. Li, W. Zhu, T. Liu, J. Zhao and L. Gao, *J. Mater. Chem. A* 2021, **9**, 11827-11838.
12. C. Guo, J. Yang, Z. Cui, S. Qi, Q. Peng, W. Sun, L.-P. Lv, Y. Xu, Y. Wang and S. Chen, *Journal of Energy Chemistry*,

2022, **65**, 514-523.